nature biomedical engineering

ARTICLES

https://doi.org/10.1038/s41551-020-00661-1

Check for updates

A fluorescence sandwich immunoassay for the real-time continuous detection of glucose and insulin in live animals

Mahla Poudineh[1,13], Caitlin L. Maikawa[2,13], Eric Yue Ma[1], Jing Pan[1], Dan Mamerow[3], Yan Hang[4], Sam W. Baker[5], Ahmad Beirami[6], Alex Yoshikawa[7], Michael Eisenstein[1,8], Seung Kim[4], Jelena Vučković[1,9], Eric A. Appel[2,8,10] ✉ and H. Tom Soh[1,11,12] ✉

Biosensors that continuously measure circulating biomolecules in real time could provide insights into the health status of patients and their response to therapeutics. But biosensors for the continuous real-time monitoring of analytes in vivo have only reached nanomolar sensitivity and can measure only a handful of molecules, such as glucose and blood oxygen. Here we show that multiple analytes can be continuously and simultaneously measured with picomolar sensitivity and sub-second resolution via the integration of aptamers and antibodies into a bead-based fluorescence sandwich immunoassay implemented in a custom microfluidic chip. After an incubation time of 30 s, bead fluorescence is measured using a high-speed camera under spatially multiplexed two-colour laser illumination. We used the assay for continuous quantification of glucose and insulin concentrations in the blood of live diabetic rats to resolve inter-animal differences in the pharmacokinetic response to insulin as well as discriminate pharmacokinetic profiles from different insulin formulations. The assay can be readily modified to continuously and simultaneously measure other blood analytes in vivo.

Technologies that can continuously measure circulating biomolecules in vivo would have a transformative impact towards the vision of precision medicine[1]. Such tools could provide valuable insights into the health status of patients and their response to therapeutics, thereby allowing clinicians to tailor therapeutic regimens to consistently deliver maximum efficacy with minimal side-effects even when there is considerable variability in pharmacokinetics and pharmacodynamics across patient populations. Early efforts towards this end have already had a considerable impact—for example, continuous glucose monitors have greatly reduced the burden for diabetes patients and increased the time during which the blood glucose levels of a patient are within the euglycaemic range[2]. Similar monitoring could prove invaluable for managing a host of other disease states[3–6]. Unfortunately, it remains exceedingly difficult to achieve continuous in vivo detection of biomolecules and continuous real-time sensors have to date been limited to only a handful of analytes such as glucose[7], lactate[8] and blood oxygen[9].

A new generation of biosensors has recently emerged that can continuously measure other types of biomolecules in vivo. For example, our group demonstrated continuous detection of small-molecule drugs in the bloodstream of live animals using an electrochemical sensor based on structure-switching aptamer probes[10]. Similar strategies have enabled multi-hour monitoring of four drugs (doxorubicin, kanamycin, gentamicin and tobramycin) in blood[11]. These technologies represent notable advances in terms of demonstrating the feasibility of continuous in vivo molecular detection, but such approaches have been limited in sensitivity. These early biosensors can only measure target molecules at relatively high concentrations (typically in the high nanomolar to micromolar range) and cannot measure other clinically important analytes that exist at lower (for example, picomolar) concentrations[12].

Insulin is one of the most important therapeutic molecules, with over 50 million patients with diabetes worldwide requiring insulin replacement therapy[13–15]. Accurate insulin dosing is critical because excess insulin can result in acute hypoglycaemia, which can lead to dangerously—and potentially fatally—low blood-sugar levels[16,17]. A study conducted in 2015 estimated that consequences of insulin administration-related errors by patients account for more than 97,000 hospital visits annually in the US[18]. Furthermore, it is well known that patients have diverse responses to insulin and that insulin absorption and clearance rates can differ dramatically between patients—or even in the same patient—depending on factors such as temperature, preparation technique and injection site[19–21]. However, measurement of the insulin kinetics for individual patients requires frequent blood draws and subsequent laboratory analysis, which is not practically feasible and is thus not a component of standard clinical practice. Treatment regimens are instead planned based on modelled population data and include an element of trial and error due to the above-mentioned inter-individual variability. Thus, the ability to continuously measure in vivo insulin and glucose concentrations with a simple and relatively low-cost device would be highly

[1]Department of Electrical Engineering, Stanford University, Stanford, CA, USA. [2]Department of Bioengineering, Stanford University, Stanford, CA, USA. [3]Department of Chemical Engineering, University of California, Santa Barbara, Santa Barbara, CA, USA. [4]Department of Developmental Biology, Stanford University, Stanford, CA, USA. [5]Department of Comparative Medicine, Stanford University, Stanford, CA, USA. [6]Research Laboratory of Electronics, Massachusetts Institute of Technology, Cambridge, MA, USA. [7]Department of Chemical Engineering, Stanford University, Stanford, CA, USA. [8]Department of Pediatrics (Endocrinology), Stanford University, Stanford, CA, USA. [9]Ginzton Lab, Stanford University, Stanford, CA, USA. [10]Department of Materials Science and Engineering, Stanford University, Stanford, CA, USA. [11]Department of Radiology, Stanford University, Stanford, CA, USA. [12]Chan Zuckerberg Biohub, San Francisco, CA, USA. [13]These authors contributed equally: Mahla Poudineh, Caitlin L. Maikawa. ✉e-mail: eappel@stanford.edu; tsoh@stanford.edu

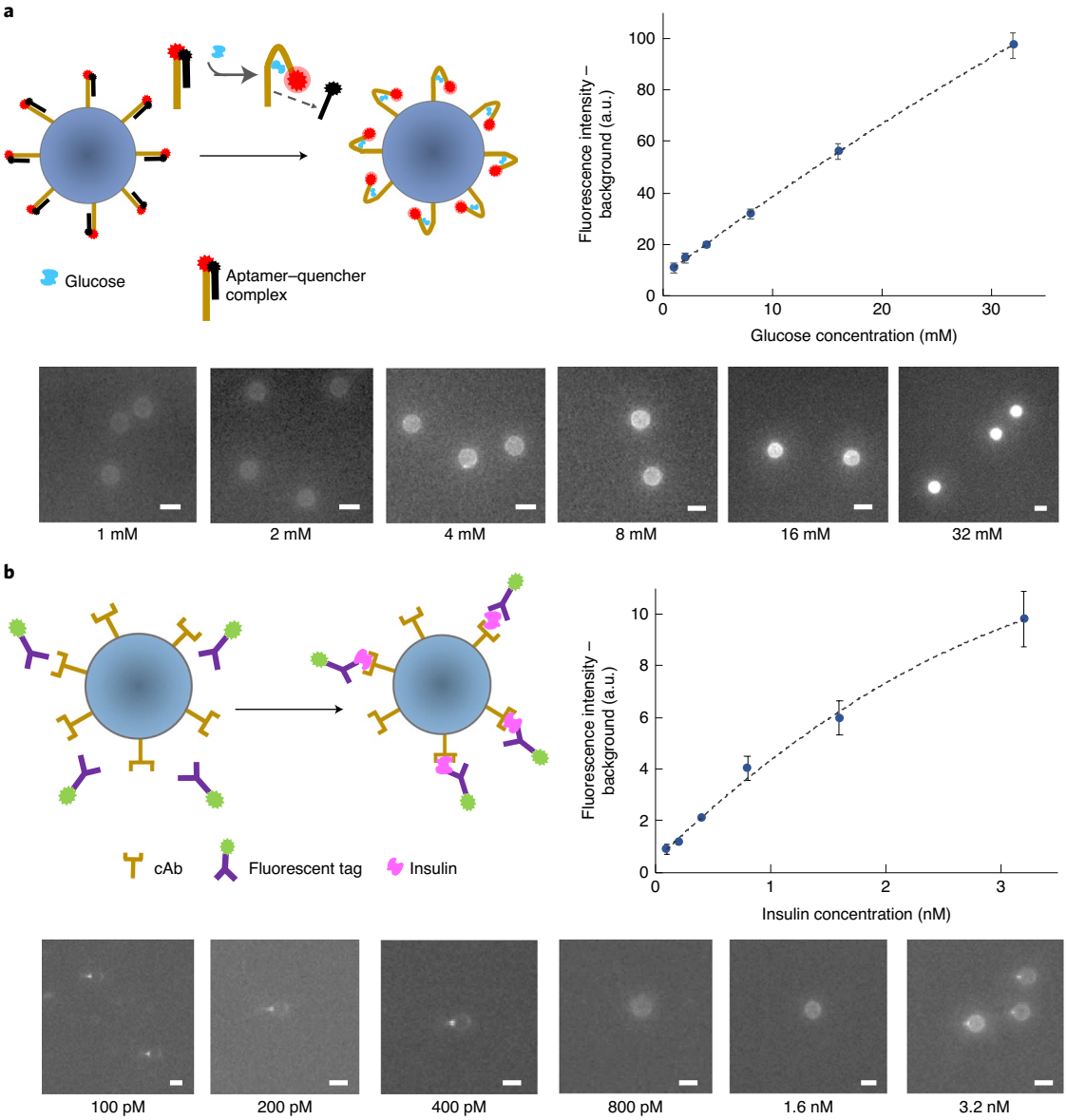

Fig. 1 | Overview and validation of the RT-ELISA assay strategy. The RT-ELISA employs two parallel assays to track transient changes in the glucose and insulin levels. **a**, Microbeads (15 μm) are functionalized with a glucose aptamer conjugated with Cy5 fluorophore, which is hybridized to a DNA competitor conjugated to a quencher (BHQ2). In the presence of glucose, the competitor strand is displaced, thereby eliminating quenching and producing a fluorescent signal (top left). For the glucose-probe validation, microbeads functionalized with the aptamer–competitor complex were incubated with different concentrations of glucose in buffer. After an hour, the beads were washed three times and imaged with a red laser to excite the Cy5 fluorophore (bottom). The fluorescence signal intensity at each concentration is shown (top right; 11 ± 2, 15 ± 2, 20 ± 1, 32 ± 2, 56 ± 3 and 97 ± 5). **b**, Insulin is detected in a sandwich assay with microbead-conjugated cAbs and R-PE-tagged dAbs (top left). For the insulin-probe validation, microbeads functionalized with the cAbs were incubated with different concentrations of insulin and R-PE-labelled dAbs. After an hour, the beads were washed three times and imaged with a green laser to excite the R-PE fluorophore (bottom). The fluorescence signal intensity at each concentration is shown (top right; 0.9 ± 0.2, 1.2 ± 0.1, 2.1 ± 0.1, 4 ± 0.5, 6 ± 0.7 and 10 ± 1.1). In **a** and **b**, at least ten beads were measured for each concentration; the error bars show the s.d. between the beads. Nonlinear regression analysis was used for curve-fitting. Scale bars, 15 μm. a.u., arbitrary units.

valuable, enabling clinicians to create optimal therapeutic regimens that are tailored to individual diabetic patients.

To this end, we report a biosensor system that can continuously and simultaneously measure the physiological levels of circulating glucose and insulin in vivo with picomolar sensitivity and sub-second temporal resolution. Our 'real-time enzyme-linked immunosorbent assay' (RT-ELISA) technology integrates aptamer- and antibody-based molecular probes into a bead-based fluorescence assay wherein analyte concentrations are measured with a highly sensitive optical readout using a specially designed microfluidic chip. Here we demonstrate the capability to simultaneously measure clinically relevant concentrations of both insulin and glucose in the blood of live diabetic rats. Importantly, we were able to clearly discriminate inter-individual differences in the pharmacokinetic and pharmacodynamic responses to insulin. Our system is also able to distinguish the clear pharmacokinetic differences between different formulations of insulin, which were specifically developed for short- and long-acting time profiles.

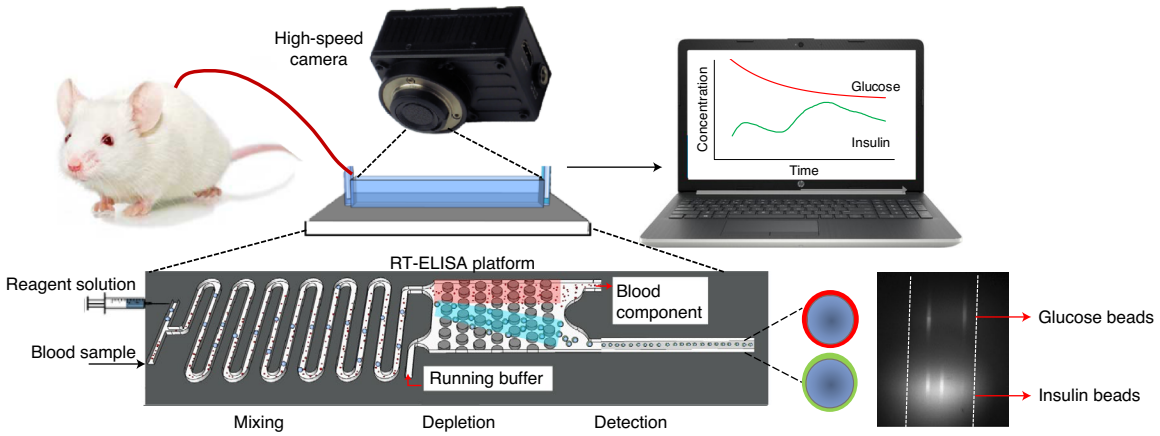

Fig. 2 | Overview of the RT-ELISA technology. The biosensor is connected to a rat through an angio-catheter, with blood injected into the device using a peristaltic pump. The device consists of three modules: a mixing module where blood is combined with the detection reagents (which are introduced to the device via a syringe pump), a depletion module for eliminating excess blood cells and a detection module that transfers the fluorescently labelled beads to the detection window.

Results and discussion

RT-ELISA detection strategy. The RT-ELISA employs two different bead-based target capture strategies to detect both insulin and glucose in parallel. For glucose, we used aptamer probes and a strand-displacement strategy[22–24]. Briefly, we hybridized Cy5 fluorophore-conjugated glucose aptamers[25] with a DNA competitor strand that was conjugated to a quencher (BHQ2) molecule and coupled these complexes to polystyrene microbeads. The aptamer–DNA competitor complex keeps the fluorophore and quencher in close proximity, producing no signal in the absence of target. When the aptamer binds to glucose, the competitor strand dissociates and alleviates quenching of the fluorophore, producing a signal (Fig. 1a, left). For insulin, we developed a fluorescence-based sandwich immunoassay in which microbeads were functionalized with anti-human insulin antibodies as capture reagents, with detection achieved with a second anti-insulin antibody labelled with R-phycoerythrin (R-PE; Fig. 1b, left).

We initially validated the performance of our glucose and insulin assays in buffer. After functionalizing microbeads with the aptamer–DNA competitor complex for glucose detection or insulin capture antibodies (cAbs), we incubated the beads with different concentrations of glucose (Fig. 1a) or insulin plus detection antibodies (dAbs; Fig. 1b). After an hour we were able to detect bead–target complexes under a fluorescence microscope. We estimated the limit of detection (LOD) of our assay to be three times the standard deviation of the fluorescence signal intensity from a blank sample (see Methods). We achieved an LOD of 3.2 mM and 170 pM for glucose and insulin, respectively. For patients without diabetes, the secreted insulin concentrations are typically about 40 pM when fasting and increase to over 500 pM following meals[26,27]. Peak insulin concentrations in patients with diabetes can be more variable; the typical peak insulin concentrations after a prandial bolus are between 200–600 pM in patients with type 1 diabetes, depending on the dose[28,29]. Glucose levels rarely deviate from between 3.5 and 8.0 mM in patients without diabetes but concentrations can rise to >20 mM after meals in patients with diabetes if insulin is not given[27,30]. Based on these metrics, our assay can achieve sufficient sensitivity to measure physiologically relevant concentrations of glucose and insulin in diabetic patients.

RT-ELISA device testing and optimization. The RT-ELISA device integrates three modules to achieve continuous real-time monitoring: (1) a mixing module, which combines molecular probes for analyte detection with the whole-blood sample; (2) a depletion module, which minimizes background by reducing the number of blood cells in the sample; and (3) a detection module, which brings the target to the detection window to quantitatively measure its abundance (Fig. 2).

We used a standard microfluidic device fabrication protocol with glass substrates and polydimethylsiloxane (PDMS) to build the RT-ELISA device. Before fabricating the full device, we first optimized the individual mixing, depletion and detection modules. The mixing module achieves rapid and continuous mixing of reagents through the use of serpentine channels with an optimized length and incorporates herringbone structures inside the channel[31,32] (Fig. 3a, bottom). This dramatically enhances the rate of molecular diffusion and reduces the required incubation time to less than one minute. We injected different concentrations of insulin into the mixing module through the sample inlet and injected a solution of fluorescently tagged dAbs and microbeads functionalized with the insulin cAb through the reagent inlet. We injected these solutions at different flow rates, and then collected the beads from the module outlet and observed them under a fluorescence microscope (Supplementary Fig. 1). No aggregation of insulin or the dAb were observed under operating conditions (Supplementary Figs. 2 and 3). After comparing the fluorescence signal intensity obtained at different flow rates with the intensity achieved with standard bench-top incubation (Fig. 3a, top), we found that optimal mixing occurs at a flow rate of 15 μl min^{-1}, with a total mixing time of 30 s. At lower flow rates, the herringbone structures do not produce perturbation and chaotic mixing efficiently, resulting in low mixing efficiency. In contrast, there is insufficient time for the reagents to be mixed together at higher flow rates. It should be noted that the RT-ELISA system does not operate under equilibrium conditions (Supplementary Fig. 4) but we emphasise that this does not change the effectiveness of our system. As long as the output signal is consistently proportional to the analyte concentration, it is not necessary to reach equilibrium to quantitatively determine the analyte concentrations. Many widely used assays operate under non-equilibrium conditions, including digital ELISA[33–35].

The depletion module was designed to not only eliminate blood cells but also free fluorescently tagged antibodies, thereby reducing the background (Supplementary Video 1). This module (Fig. 3b) employs deterministic lateral displacement (DLD) sorting to isolate beads from blood cells. DLD is an established hydrodynamic approach for separating particles based purely on size in a continuous manner[36]. DLD utilizes specific arrangements of posts in a channel to facilitate the separation of particles that are either

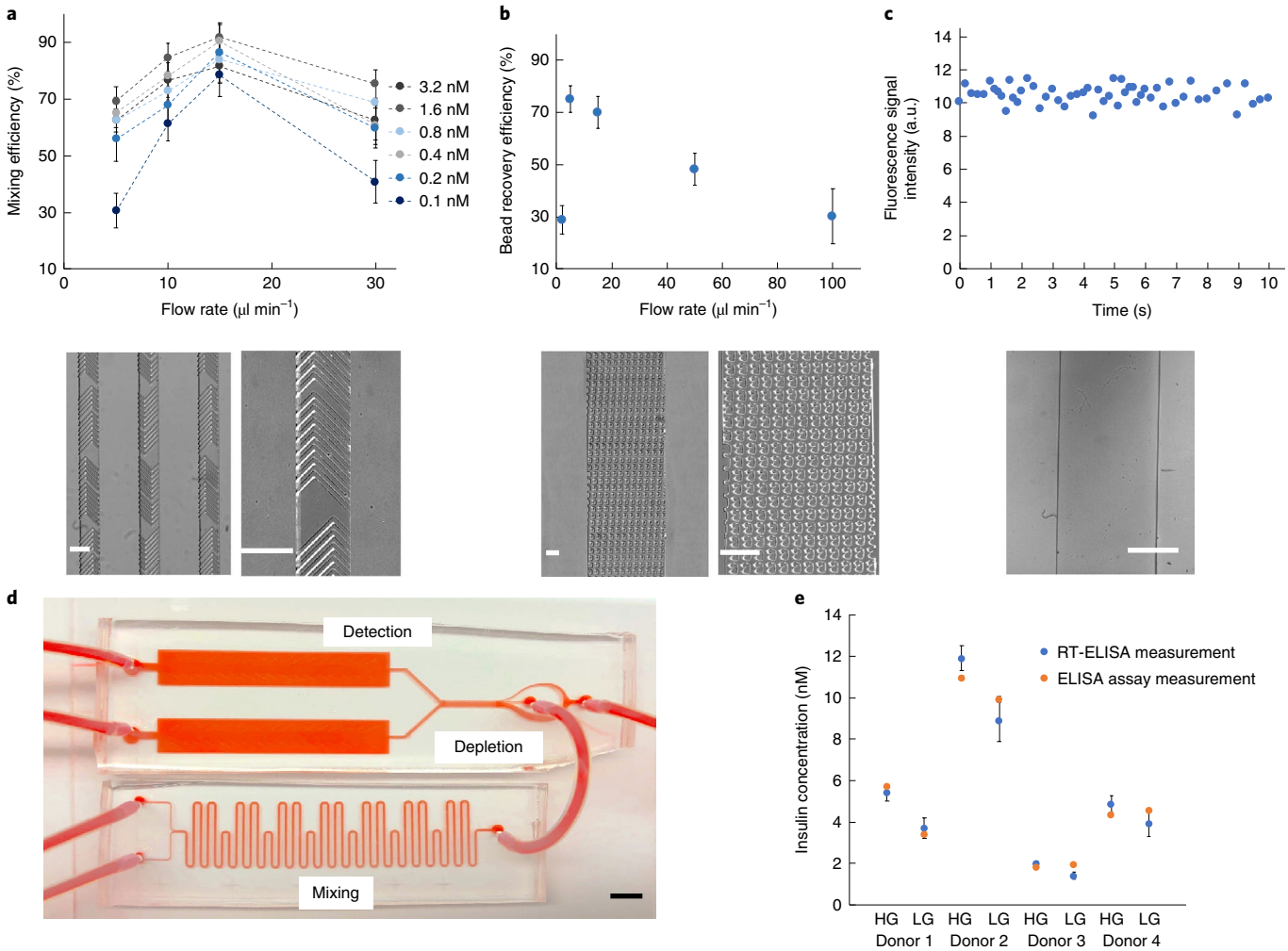

Fig. 3 | Testing and optimization of the core components of RT-ELISA. a, Optimization of the performance of the mixing module. We injected different concentrations of insulin and detection reagents through their respective inlets at different flow rates. We then collected the beads and observed their fluorescence signal under a microscope relative to a detection reaction with a standard bench-top incubation of 2 h (top; 31 ± 6, 61 ± 6, 79 ± 8 and 41 ± 8 for 0.1 nM insulin; 56 ± 8, 68 ± 7, 87 ± 4 and 60 ± 7 for 0.2 nM insulin; 65 ± 6, 78 ± 3, 90 ± 8 and 61 ± 7 for 0.4 nM insulin; 63 ± 5, 73 ± 6, 84 ± 6 and 69 ± 7 for 0.8 nM insulin; 69 ± 4, 85 ± 8, 92 ± 6 and 75 ± 8 for 1.6 nM insulin; 63 ± 4, 77 ± 6, 82 ± 6 and 63 ± 7 for 3.2 nM insulin). The experiment was performed three times. Images of the mixer device with serpentine channel and herringbone structures (bottom). **b**, Optimization of the performance of the depletion module. We spiked whole blood with 15-μm microbeads and tested the performance of the notched post structures for bead recovery and blood-cell depletion at different flow rates (top; 28 ± 5, 75 ± 5, 70 ± 6, 48 ± 6 and 30 ± 10). The experiment was performed three times. Images of the depletion module are shown (bottom). **c**, Optimization of the performance of the detection module and assessment of the temporal resolution. We introduced fluorescently labelled microbeads into the detection module and observed the beads over 10 s. We measured an average of five beads passing through the detection window every second, which defines a temporal resolution of 200 ms (top). Image of the detection window is shown (bottom). a.u., arbitrary units. **d**, The fully integrated RT-ELISA device. **e**, Insulin probes were incorporated into the device and used to measure endogenous insulin secreted from human islet samples after a glucose challenge at high (HG) or low (LG) concentrations. The RT-ELISA readout was compared with conventional ELISA (RT-ELISA measurements: 5.4 ± 0.7, 3.7 ± 0.5, 11.9 ± 0.6, 8.9 ± 1, 2 ± 0.1, 1.4 ± 0.2, 4.9 ± 0.6 and 3.9 ± 0.6; ELISA assay measurements: 5.7 ± 0.1, 3.4 ± 0.2, 11 ± 0.2, 9.9 ± 0.1, 1.8 ± 0.1, 1.9 ± 0.2, 4.3 ± 0.1 and 4.6 ± 0.2). The experiment was performed three times with human islets from four donors. Scale bars, 150 μm (**a**–**c**) and 5 mm (**d**). The error bars depict the s.d.

larger or smaller than a critical diameter by precisely controlling their trajectory in the device. In this scenario, the critical diameter is 15 μm, based on the diameter of the microbeads used for target capture, and we sought to design a device that would allow us to isolate these beads amid a far larger number of blood cells, which are smaller than 15 μm. We tested the notched[37] post structures (see the 'Depletion module design' section of Methods for details) and introduced a sheath buffer solution into the device along with the sample for bead recovery and blood-cell depletion. We achieved the best performance (both for bead recovery and blood-cell depletion) at a sample flow rate of 5–20 μl min^{-1} and a sheath buffer-to-sample flow rate ratio of 5:1 (Fig. 3b (top) and Supplementary Figs. 5,6). The depletion performance worsened at higher or lower inlet flow rates.

In the detection module, the target-bound beads flow into a detection window (Fig. 3c, bottom) and their fluorescence intensity is continuously measured with a high-speed camera under spatially multiplexed two-colour laser illumination (see Methods and Supplementary Information). Incoming beads are first illuminated by a red laser, which interrogates the Cy5 fluorescence intensity indicating the glucose concentration. This is followed by illumination with a green laser that interrogates the R-PE fluorescence intensity, which measures the insulin concentration. We

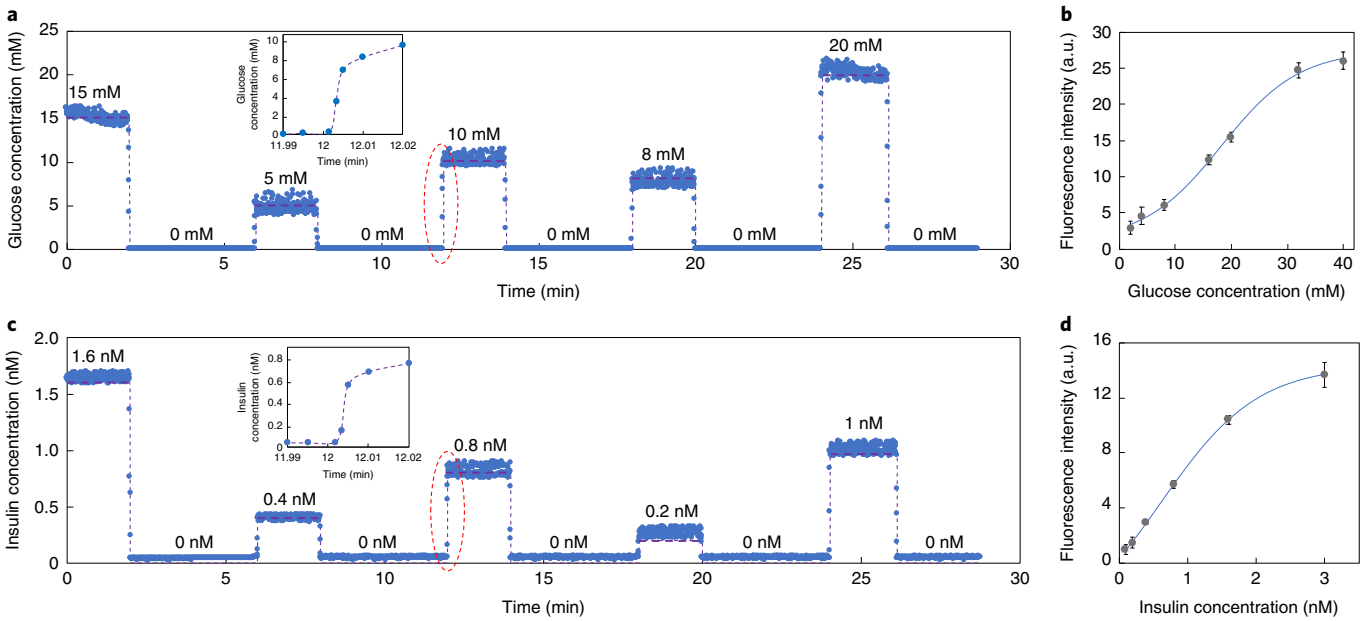

Fig. 4 | Continuous in vitro monitoring of glucose and insulin in whole blood. a,**c**, RT-ELISA measurements of glucose (**a**) and insulin (**c**) in human whole blood (blue dots) relative to the actual concentrations (purple dashed line) over the course of 30 min. Insets: RT-ELISA readout at a higher temporal resolution, where the glucose and insulin concentrations are introduced at $t = 12$ min (red ovals). **b**,**d**, Standard curves correlating the fluorescence signal intensity to the glucose (**b**) and insulin (**d**) concentrations (**b**: 2.9 ± 1, 4.6 ± 1.2, 6.1 ± 0.8, 12.3 ± 0.7, 15.5 ± 0.7, 24.7 ± 1.1 and 26 ± 1.2; **d**: 0.9 ± 0.5, 2 ± 0.2, 3.2 ± 0.4, 5.9 ± 0.3, 10.7 ± 0.2 and 13.7 ± 0.5). The experiments to derive the standard curves were repeated three times and the error bars show the s.d.; a.u., arbitrary units. Nonlinear regression analysis was used for curve-fitting. Data reflect individual bead readouts, where at least 200 beads were measured for each concentration. Incubation was performed in the mixing module for a total of 30 s. The RT-ELISA system possesses an intrinsic delay due to the time that bead–target complexes spend in the mixing module (30 s), in the tube connecting the mixing and DLD modules (100 s) and in the DLD module (<1 s). We accounted for this total delay time (approximately 130 s) in our results. Measurements were performed for 2 min; buffered solution was injected into the device for 4 min between the sample changes. The fluorescence signal intensity from a blank blood sample was measured to quantify the endogenous insulin and glucose. For the insulin measurements, the fluorescence signal intensity from the blank was subtracted from the measured signal at each concentration. Note that the endogenous insulin concentration in the blood was significantly lower than all concentrations measured during subsequent experiments and we therefore neglected the endogenous component when generating the calibration curve. For the glucose measurements, endogenous glucose was measured using a conventional glucose meter and subtracted as the baseline before calculating the spiked concentrations.

used an exposure time of 50 ms and acquired images every 100 ms (Supplementary Video 2). We introduced fluorescently labelled microbeads into the detection module at an inlet flow rate of 15 µl min^{-1} and measured the fluorescence signal intensity as well as the number of beads passing through the detection window over a short time scale. We observed an average of five beads passing through the detection window every second, indicating a temporal resolution of approximately 200 ms (Fig. 3c, top). The fast frame rate and high sensitivity of the camera allowed us to continuously track individual microbeads, enabling quantitative detection of analytes in real time. Finally, we combined the three modules to produce the integrated RT-ELISA device (Fig. 3d). To achieve this, we simulated and adjusted the fluidic resistance between the different modules. The process used to generate the fully integrated device is described in Methods and Supplementary Figs. 6–9. We also compared the integrated mixing and depletion modules in RT-ELISA with bench-top incubation (Supplementary Fig. 10).

Next, we tested the RT-ELISA device to detect endogenous, secreted human insulin[38]. We treated intact human islets with culture medium containing low (2.8 mM) and then high (16.7 mM) concentrations of glucose to stimulate insulin secretion in vitro. The supernatants were collected after each stimulation and the insulin concentration was measured using both the RT-ELISA device and conventional ELISA. We performed this experiment using islets from four different donors. The results presented in Fig. 3e show that our bead-based assay is capable of measuring endogenous human insulin levels and that the measurements obtained from our device closely matched those from the ELISA assay (Supplementary Fig. 11).

Continuous measurement of glucose and insulin in whole blood. To characterize the sensitivity and temporal resolution of the RT-ELISA device, we tested it with human whole blood spiked with known concentrations of glucose and insulin (Fig. 4). We used these data to construct standard curves that correlate the fluorescence signal intensity with the glucose or insulin concentration in whole blood (Fig. 4b,d). The experiments used to derive these standard curves were repeated three times (replicates shown in Supplementary Figs. 12 and 13).

We developed custom software to continuously measure the fluorescence signal intensity and quantify the glucose and insulin concentrations (see Methods). Our device achieved an LOD of 3.7 mM for glucose and 109 pM for insulin measurements in blood. The LOD for insulin using the RT-ELISA device was considerably lower than that for the bench-top assay (Fig. 1b), and this improved sensitivity is due to the efficient elimination of free bound antibodies in the DLD module compared with the washing in the bench-top bead assay. Fasting insulin in patients without diabetes (approximately 40 pM) is below this limit, but an LOD of 109 pM is sufficient to track the pharmacokinetics of post-prandial insulin. Although the LOD for glucose will need to be further optimized to detect hypoglycaemia (LOD = 2.2 mM)[39], our glucose detection limits cover both the euglycaemic and the relevant hyperglycaemic ranges. We then introduced different concentrations of glucose and insulin

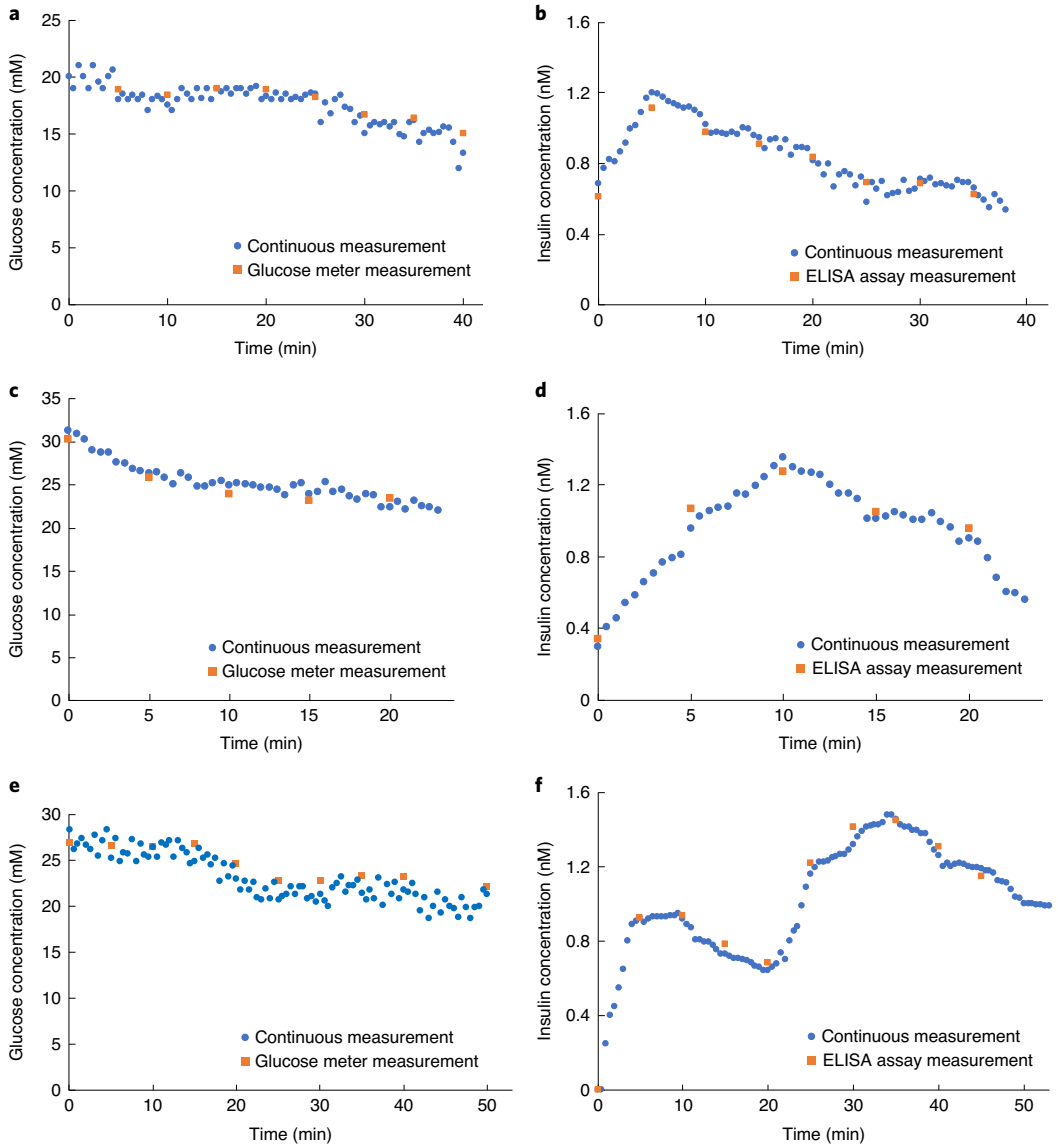

Fig. 5 | Continuous real-time measurements of glucose and insulin in diabetic rats. a–f, RT-ELISA measurement of in vivo glucose (**a**,**c**,**e**) and insulin (**b**,**d**,**f**) concentrations over 30–50 min in three different rats. Diabetic rats were injected subcutaneously with a single bolus (at $t = 0$ min; **a**–**d**) or two boluses (at $t = 0$ and 20 min; **e**,**f**) of Humulin R (1 U kg^{-1}). Each blue dot shows the median RT-ELISA readout of individual bead (approximately 150 beads) measurements over 30 s. For comparison, we collected blood samples from the tail vein every 5 min and measured the glucose and insulin levels using a hand-held glucose meter and conventional ELISA, respectively. These results correlated closely and highlight the inter-individual variability in the insulin response. For the RT-ELISA, incubation was performed in the mixing module for a total of 30 s. Note that in this experiment there is a 5 min external delay from the tube connecting the device to the rat, in addition to the intrinsic RT-ELISA delay (130 s).

to whole-blood samples and used the RT-ELISA device to monitor these analytes for approximately 30 min (Fig. 4). The measured concentrations differed from the known concentration by an average of 250 μM and 24 pM for the glucose and insulin measurements, respectively, over the course of the experiment. This standard deviation is sufficiently small for our system to be employed to reliably quantify glucose and insulin in patients with diabetes, where the post-prandial concentrations are typically more than 3.5 mM and 300 pM, respectively.

Continuous glucose and insulin measurements in vivo. Having demonstrated the ability of our technology to sensitively and accurately detect insulin and glucose in vitro, we evaluated its performance in vivo in a streptozotocin-induced rat model of insulin-deficient diabetes[40]. We chose this model because it lacks endogenous insulin, thus eliminating the potential of background due to antibody cross-reactivity. The device was connected to an anaesthetized rat by a femoral venous catheter (Supplementary Fig. 14). Humulin R (recombinant human insulin) boluses were given at one ($t = 0$ min) or two ($t = 0$ and 20 min) time points, while continuous real-time monitoring of the glucose (Fig. 5a,c,e) and insulin (Fig. 5b,d,f) levels was performed over the course of 30–50 min. In experiments monitoring only a single insulin bolus (Fig. 5a,c), the baseline insulin measurements were elevated due to insulin boluses given 40 min before the experiment. The peak insulin concentrations were detected at either 5 min (Fig. 5b) or 10 min (Fig. 5d) after single insulin injections. After two successive bolus injections, the peak insulin concentrations were observed at 10 and 35 min (Fig. 5d). In parallel, we compared the RT-ELISA results with conventional ELISA analyses of insulin in blood samples collected from the rat

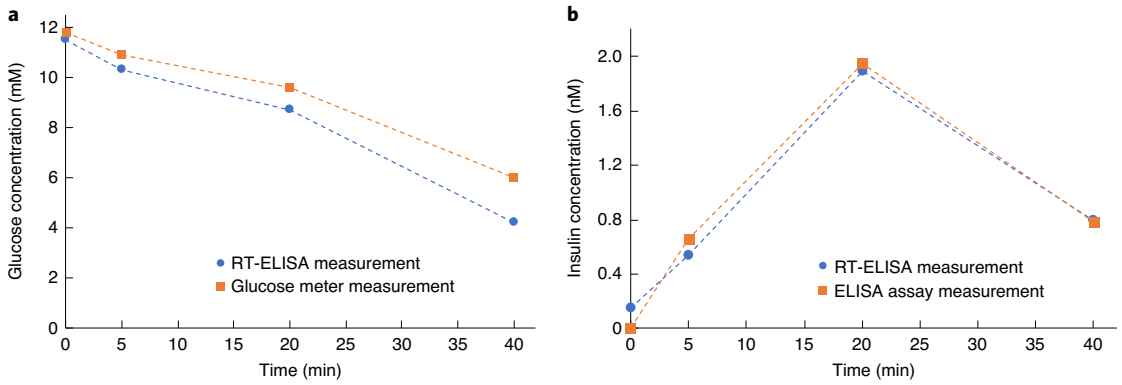

Fig. 6 | Glucose and insulin measurements in an awake diabetic rat. a,**b**, An awake diabetic rat was injected with human insulin and blood samples were collected at $t = 0$, 5, 20 and 40 min after injection. Glucose levels were measured using RT-ELISA and a glucose meter (**a**), and insulin levels were measured using RT-ELISA and ELISA assay (**b**). RT-ELISA measurements were collected using the average of continuous flow measurements in the device (incubation time = 30 s) from the blood samples collected at each time point.

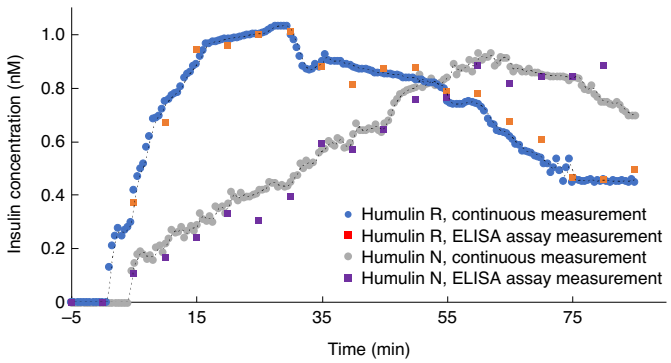

Fig. 7 | Comparison of different insulin formulation pharmacokinetics. Diabetic rats were injected with either Humulin R (1 U kg^{-1}; $n = 1$ rat) or Humulin N (2 U kg^{-1}; $n = 1$ rat) and their insulin concentrations were monitored using RT-ELISA and ELISA. The RT-ELISA incubation time was 30 s; as in Fig. 5, there was a 5 min external delay from the tubing connecting the device to the rat in addition to the intrinsic RT-ELISA delay (130 s).

tail vein every 5 min and glucose measurements from a hand-held glucose monitor, and observed a close correlation between both sets of results (Supplementary Fig. 15). The differences between peak insulin action in individual rats clearly show the variability in insulin pharmacokinetics, even under controlled conditions with genetically similar animals. This has important implications for human patients, who are genetically diverse, use different injection sites and have different environmental conditions, exacerbating this inter-individual variability. Thus, these results highlight the necessity of personalized insulin monitoring.

We observed that the insulin dose used in our experiments was insufficient to decrease the blood glucose concentrations to normoglycaemic conditions. However, we have demonstrated that the observed decrease in blood glucose after insulin administration in our anaesthetized rats is comparable to blood-glucose depletion in a conscious rat. We administered the same insulin dose (1 U kg^{-1}) to a conscious rat and collected blood samples at $t = 0$, 5, 20 and 40 min after injection. We then employed the RT-ELISA device to measure the glucose (Fig. 6a) and insulin (Fig. 6b) levels. We observed a decrease in the glucose concentrations in both the glucose meter measurements and the RT-ELISA device, with a 7 mM decrease in the glucose level after 40 min. These results are comparable to the results from the continuous monitoring experiments and corroborate the expected effect of a 1 U kg^{-1} insulin bolus on glucose concentrations.

Continuous in vivo tracking of different insulin formulations. There are both short- and long-acting commercially available recombinant insulin formulations, which exhibit different absorption kinetics after injection. We have found that RT-ELISA can differentiate the pharmacokinetics of these formulations, based on experiments comparing the kinetics of Humulin R and Humulin N (neutral protamine Hagedorn insulin). Humulin R is considered a short-acting insulin, whereas Humulin N was developed to achieve delayed onset and extended duration of action as an early basal-insulin replacement[41–43].

After measuring the baseline concentrations for 5 min, diabetic rats were injected with Humulin R or Humulin N and the glucose and insulin concentrations were quantified over the course of 85 min (Fig. 7 and Supplementary Fig. 16). The different pharmacokinetics of Humulin R and Humulin N were clearly evident in the RT-ELISA measurements, with these two formulations producing peaks at approximately 15 and 60 min, respectively, after injection.

Outlook

We have demonstrated that the RT-ELISA device can achieve sensitive and accurate continuous monitoring of insulin and glucose in the circulating blood of live animals, thereby enabling real-time in vivo analysis of insulin pharmacokinetics and pharmacodynamics. Experiments in human blood demonstrated that our sensor achieved sufficient sensitivity to detect clinically relevant concentrations of both analytes, with an LOD of 3.7 mM for glucose and 109 pM for insulin. Subsequent experiments in anaesthetized diabetic rats confirmed our capacity to continuously monitor in vivo changes in insulin and glucose in real time and highlighted the ability of the RT-ELISA technology to distinguish clear inter-individual differences in the pharmacokinetics of insulin—a critical feature for clinical implementation. Importantly, the RT-ELISA measurements closely matched those obtained with standard ELISA and clinical glucose sensors. We noted with both readouts that the use of isoflurane anaesthesia impeded the response of rats to insulin but subsequently confirmed our ability to accurately track insulin-induced changes in circulating glucose with samples collected from awake rats at multiple time points. Finally, we demonstrated the capability to accurately discriminate the distinct pharmacokinetic profiles associated with two different insulin formulations, short-acting Humulin R and intermediate-acting Humulin N.

There have been recent advancements in rapid biomarker -measurement technologies but these technologies are usually single-time-point assays that require lengthy incubation times and are thus unsuitable for real-time continuous detection. Most of the wearable and continuous sensing devices available at present are limited to the measurement of analytes in sweat or processed blood plasma[44–47]. In contrast, RT-ELISA offers the powerful capability to achieve high-resolution continuous protein monitoring directly in whole blood with picomolar sensitivity. To allow for real-time analysis, RT-ELISA requires a continuous supply of reagents, which corresponds to approximately US$10.50 worth of reagents consumed for a 1-h run (Supplementary Table 1). The next steps for the development of RT-ELISA will focus on expanding the detection range to encompass glucose levels in the hypoglycaemic range and basal levels of insulin, which would extend the utility for RT-ELISA beyond understanding insulin bolus pharmacokinetics to applications including artificial pancreas control and basal-insulin sensing. It may be advantageous to expand the range of RT-ELISA analytes in future work to include lactate or cortisol, which could prove valuable during periods of high-intensity exercise and enable the use of data from these intervals to inform changes in insulin dosing to prevent hypoglycaemia[48–50]. Although it is beyond the scope of this work, we believe our system could be readily modified for human use. Before translation, the system would have to be optimized for safety; this would include measures such as incorporating one-way valves to ensure no backflow of reagents into the patient as well as careful preparation of the tubing and chip surface with anticoagulants to avoid clotting. The detection scheme will also need to be miniaturized to reduce its complexity, most notably with regard to the camera and other optical components. However, we believe that such miniaturization would be possible with integrated photonics and that further advances in these technologies could make RT-ELISA suitable for bedside patient monitoring. With such modifications, RT-ELISA could provide the foundation for a clinically useful assay for the development of personalized insulin therapy regimens for individual patients and it could also serve as a valuable research tool to assess the pharmacokinetics and pharmacodynamics of novel insulin formulations for both preclinical testing and clinical trials.

Although in this work we demonstrate the simultaneous detection of two analytes, we believe that higher levels of multiplexing can be achieved with a more advanced optical design. Finally, we would like to emphasise that the RT-ELISA system is a versatile technology that could be readily modified to continuously measure other circulating analytes in vivo, for which aptamers or antibody pairs are available, thus potentially making it a broadly applicable tool for biomedical research.

Methods

Materials. All chemicals were purchased from Sigma-Aldrich, unless otherwise noted. SuperAvidin-coated microspheres (15 μm) were obtained from Bangs Laboratories, human whole blood was obtained from BioIVT and matched paired insulin antibodies (capture, BM364-Z8A2; and detection, BM364-T8F5) were obtained from BBI Solutions. Insulin antibodies were validated using a bench-top bead-based assay for use in the RT-ELISA device. Human insulin was obtained from R&D Systems, streptozotocin (STZ) was obtained from MedChem Express, Humulin R and Humulin H were obtained from Eli Lilly, the R-PE antibody conjugation kit was obtained from Thermo Fisher Scientific, and the glucose aptamer and DNA competitor oligonucleotides were ordered from Integrated DNA Technologies.

The glucose aptamer sequence used was 5′-/5Biosg/iCy5/CTCTCG GGACGACCGTGTGTGTTGCTCTGTAACAGTGTCCATTGTCG TCCC-3′, where 5Biosg indicates a biotin modification at the 5′ end and iCy5 is Cy5 labelling at the 5′ end. The DNA competitor strand was 5′-GGTCGTCCCGAGAG/3BHQ2/-3′, where BHQ is a black-hole quencher.

RT-ELISA device fabrication. A PDMS (Dow Chemical) device fabrication protocol was employed. First, two silicon masters were fabricated: one for the mixing module and one for the depletion and detection modules. Masks were designed using AutoCAD software (Supplementary Fig. 9) and then printed (CAD/Art Services and Advance Production). Two 50-μm layers of SU8-3050 (MicroChem) were patterned to make the mixing module master. The first layer was patterned to make the channel and the second was aligned for herringbone-structure fabrication. The depletion and detection module masters were patterned using one layer of SU8-3050 (MicroChem). After master fabrication, a mixture of PDMS and curing agent at a ratio of 10:1 was poured onto the device masters. Both masters were baked at 67 °C for 2.5 h. We then peeled the replicas and pierced holes to connect the tubing. PDMS replicas were attached to glass cover slips using a plasma treatment of 45 s and left to bond overnight. The silicone tubing (Cole-Parmer) was then attached to the inlet and outlet of the device. Before use, the devices were conditioned with 1% Pluoronic F-68 (Sigma-Aldrich) and 10% heparin (McKesson Corporation) in PBS overnight to reduce non-specific adsorption and blood coagulation.

Depletion module design. We tested the notched pillar structures in the depletion module. Pillar array positioning was calculated for the separation of particles larger and smaller than 14 μm. This cutoff was chosen to ensure maximum recovery of 15-μm microbeads while depleting the majority of blood cells, based on the critical diameter defined by the empirical formula for DLD[36]. These parameters were then relaxed by adjusting gaps according to the notched pillar shapes. The DLD arrays extended across the entire width of the device and were then trimmed in AutoCAD to create continuous walls. The sheath buffer inlet splits so that it enters along both edges of the device, ensuring that no particles or cells enter the device next to a wall. Different sample inlet-to-buffer inlet flow-rate ratios were examined, with optimal cell recovery and blood-cell depletion observed at a ratio of 1:5. Supplementary Fig. 5 shows the separation of microbeads from blood cells. Before separation, the blood-cell background blocks the signal from the beads, whereas beads can be clearly detected after separation. The optimal pillar diameter to maximize sorting efficiency in a DLD device with notched microstructures was 40 μm based on calculations described in the literature[36].

Integrated RT-ELISA device fabrication. We first connected the mixer and depletion modules and tested their performance in capturing insulin from whole-blood samples and isolating target-bound beads. As shown in Supplementary Fig. 7, blood spiked with 3 nM insulin was injected through the sample inlet at 15 μl min^{-1}, while the reagent solution containing functionalized microbeads and dAbs was injected through the reagent inlet at the same flow rate. The mixer outlet was connected to the depletion sample inlet and as the mixture entered the depletion module, a buffered solution was injected at 75 μl min^{-1} to form the required sheath flow for separation. The flow rates were optimized to achieve the best mixing efficiency, bead recovery and blood-cell depletion. The beads were collected from the depletion outlet and monitored using fluorescence microscopy. The connection of the depletion and detection modules was tested before full integration. A dummy detection module was connected to the blood-waste outlet to adjust the outlet resistance, ensuring fluid flow through the depletion device (Supplementary Fig. 8). The detection window was designed to have a width of 292 μm to accommodate the ×20 objective field used for fluorescence measurements. The detection module was then widened to 4.8 mm to prevent clogging by the high number of blood cells and beads passing through the channel. The optimized dimensions of the modules in the final device are summarized in Supplementary Table 2.

Microbead functionalization. Streptavidin-coated beads were functionalized with either monoclonal biotinylated anti-insulin cAbs or glucose aptamers hybridized with the DNA competitor strand, as directed by the bead manufacturer's recommended protocol. A typical coating procedure for 10 mg of microspheres entailed homogenizing the bead stock solution on a rotator, transferring 1 ml of the 10 mg ml^{-1} stock to a new tube, adding 10 ml of 1×PBS + 0.05% Tween 20 (PBST, pH 7.4), mixing by pipetting or vortexing, centrifuging at 2,100 r.c.f. for 5 min and removing the supernatant. The second wash was performed in the same manner. The beads were then resuspended in 20 ml of 1×PBS + 0.05% BSA + 0.01% Tween 20 (PBSBT) for insulin beads and PBSBT + 100 mM $MgCl_2$ (PBSBTMg) for the glucose beads, and incubated with 1.2 nM biotinylated cAb so that the cAb was present in excess (1.5–2 μg mg^{-1} beads) compared with the amount required to form a monolayer on the surface of each bead. The mixture was briefly vortexed or pipetted to homogeneity and incubated at room temperature on a rotator for 30 min. The beads were then pelleted via centrifugation at 2,100 r.c.f. for 5 min and washed thrice with 10 ml PBST as described above. The supernatant was removed and the beads were resuspended in PBSBT or PBSBTMg at a concentration of 10 mg ml^{-1} and stored at 4 °C until use.

Insulin fluorescence-based sandwich immunoassay. The dAb was site-specifically labelled with R-PE using a SiteClick R-PE antibody labeling kit (Thermo Fisher Scientific) according to the manufacturer's instructions. We employed the dAb conjugated with R-PE along with the bead-coupled cAbs in either a bench-top incubation or the RT-ELISA device to achieve insulin detection. For the bench-top bead assay, we incubated the beads with insulin plus dAbs. After 1 h and before imaging, we washed the beads three times by adding the washing

solution to the tubes and then removing the supernatant after centrifugation. However, we did not remove the solution completely to avoid aspirating the beads; these few remaining microlitres may contain free dAb that give rise to a high background signal.

Imaging set-up. We used a compact home-built fluorescence microscope with spatially multiplexed two-colour laser illumination and wide-field high-speed fluorescence imaging to measure the fluorescence of the beads. A Nikon CFI Plan Apo VC ×20 Air 0.75 numerical aperture ultraviolet objective was used to focus two diode lasers (520 nm/40 mW and 642 nm/5 mW) with proper excitation filters (Thorlabs) to a size of approximately 500 × 100 µm at the sample plane. The two laser spots have a spatial offset of approximately 500 µm along the bead-flow direction to enable a spatially multiplexed two-colour fluorescence readout. The entire field of view covering both spots was imaged continuously using a high-speed, high-sensitivity scientific sCMOS camera (Photometrics Prime 95B) after proper two-pass band emission filters (Chroma). Incoming beads were first illuminated by the 642-nm laser, which interrogates the Cy5 fluorescence intensity that indicates glucose detection, followed by the 520-nm laser, which interrogates the R-PE fluorescence intensity that indicates insulin concentration. To ensure that the red laser did not excite the R-PE fluorophore, we performed control experiments where only the insulin sample and its reagent solution were injected while both lasers were illuminating. We observed insulin beads passing through the green laser region, whereas no signal was observed in the red laser region. An equivalent experiment was performed for the green laser and R-PE (Supplementary Videos 3 and 4). A schematic of the imaging set-up is provided in Supplementary Fig. 17.

In vitro glucose-stimulated insulin secretion assays. De-identified human pancreatic islets were obtained from four previously healthy organ donors without diabetes through the Integrated Islet Distribution Program (http://iidp.coh.org), Alberta Diabetes Institute Islet Core and University of California San Francisco Islet Core. For each experiment, 150 primary human islets were used. Secretion assays were carried out at 37 °C in RPMI 1640 (Thermo Fisher Scientific) medium supplemented with 0.5% (vol/vol) fetal bovine serum (HyClone), 0.2% (wt/vol) BSA (Sigma-Aldrich) and D-glucose (Sigma-Aldrich) at the indicated concentrations. Briefly, the islets were incubated with a glucose concentration of 2.8 mM for two sequential 45-min incubations as an initial equilibration period, where the medium was changed after each incubation. Subsequently, the islets were challenged with 2.8 mM (low) and then 16.7 mM (high) glucose at 37 °C for 60 min. The supernatants were carefully collected at the end of the challenge for insulin quantitation using either a conventional human insulin ELISA kit (Mercodia) or RT-ELISA.

Continuous in vitro monitoring of glucose and insulin in whole blood. Human blood samples were spiked with different concentrations of glucose and insulin for in vitro tracking. Blood glucose was measured using a hand-held glucose meter (Bayer Contour Next) to calculate the spiked glucose concentrations. A reagent solution consisting of cAb-functionalized beads (4×10^3 beads ml^{-1}), PE-tagged dAbs (1 mg ml^{-1}) and glucose aptamer-capture strand complex-functionalized microbeads was prepared in PBSBTMg. Different concentrations of glucose and insulin—15 mM + 1.6 nM, 5 mM + 0.4 nM, 10 mM + 0.8 nM, 8 mM + 0.2 nM or 20 mM + 1 nM, respectively—were spiked into the whole blood and injected into the device sequentially. The spiked blood samples and the reagent solution were continuously injected through the inlets of the mixer device at a flow rate of 15 µl min^{-1}. The beads were discarded after the imaging data were collected. The reagent solution and PBSBTMg buffer were injected at a flow rate of 75 µl min^{-1}. A syringe pump (Chemyx) was used for injection. Buffered solution was injected into the device for 4 min between the sample changes. A blood sample with no spiked insulin or glucose was run through the device to measure the fluorescence signal intensity of the endogenous insulin and this was subtracted from the measured signal at each concentration. At the end of experiment, the images were collected and a custom-written program was used to measure the fluorescence signal intensity, as described in the following section. The derived standard curves were used to calculate the absolute concentrations. The experimental conditions were kept constant for all other experiments.

Image analysis. As a proxy to measure the intensity of the glucose and insulin molecules, we measured the intensity of the signal from beads passing through the detection window, which was carried out in three steps. First, we measured the background intensity. This was done by constructing an intensity profile image containing the median intensity of each pixel across all recorded frames at different time stamps. We then applied a smoothing Gaussian filter with a small 5 × 5 pixel kernel to this image to produce the background intensity. Second, we located the beads. We subtracted the background intensity from each frame and then sought connected high-intensity components within each frame. We used a tunable threshold on the intensity level to obtain a binary mask and applied a second tunable threshold to the size of the connected component to locate the beads in each frame. Finally, we computed the intensity profile over all beads and computed statistics such as mean, median and standard deviation. We exported these data into a CSV file for further processing (for example, using Excel). We also produced a video locating the beads. We determined the edges of each bead from step 2 and processed the frame to highlight the edges of the located beads. We saved all of these processed frames in a video (avi format). This provides a way to visualize the detected beads and also could be used as a way to tune the bead location thresholds in step 2. These steps were implemented in Python, and the code and Jupyter notebook for these steps and performing the images analysis are available in GitHub.

STZ-induced model of diabetes in rats. The animal studies were performed in accordance with the Guidelines for the Care and Use of Laboratory Animals and the Animal Welfare Act Regulations; all protocols were approved by the Stanford Institutional Animal Care and Use Committee. The protocol used for STZ induction was adapted from ref. [40]. Briefly, male Sprague Dawley rats (Charles River Laboratory) of 200–300 g (8–10 weeks) were weighed and fasted in the morning before treatment in the afternoon with STZ (6–8 h). The STZ was kept protected from light; immediately before administration, individual doses were diluted to 10 mg ml^{-1} in sodium citrate buffer. The STZ solution was vortexed and administered intra-peritoneally to each rat at a dose of 65 mg kg^{-1}. Water containing 10% sucrose was given to rats for 24 h after injection with STZ to prevent hypoglycaemia. The blood glucose levels of the rats were tested for hyperglycaemia daily after the STZ treatment through tail-vein blood collection using a hand-held Bayer Contour Next glucose monitor. Diabetes was defined as three consecutive blood glucose measurements >400 mg dl^{-1} in non-fasted rats.

Continuous monitoring of glucose and insulin in diabetic rats. Diabetic rats were fasted for 4–6 h. The rats were anaesthetized using 1–3% isoflurane and a 20 G catheter was inserted into the femoral vein. The catheter was then connected to a peristaltic pump (Ismatec) at a flow rate of 15 µl min^{-1}. Once the tubing was primed with blood, the device was connected and the rats were injected subcutaneously with either 1 U kg^{-1} Humulin R or 2 U kg^{-1} Humulin N. The experiments were performed over multiple days with different devices. Different rats were used for each experiment ($n = 1$ per experiment). Reagent solution was injected through the reagent inlet as the blood entered the device. The same insulin antibody pair was used for the Humulin R and Humulin N assays. Images were collected from the detection module, the fluorescence signal intensity was quantified as described above, and the glucose and insulin absolute concentrations were calculated. After injection, blood was sampled every 5 min for up to 120 min. Before injection, the baseline blood glucose was measured using a hand-held glucose meter and blood was collected in serum tubes (Starstedt) for analysis with a commercial human ELISA kit (Mercodia). We made several refinements to reduce variability and fluctuations caused by the peristaltic pump. First, we extended the length of the blood tubing compared with the reagent solution tube, increasing friction. The increase in friction raises the back pressure, which compresses the pulses together. Second, we used soft silicone tubing material, which helps absorb fluid pulsation. Note that we used the peristaltic pump only for withdrawing the blood from the rat and injecting it into the device. The DLD module is the most sensitive module as fluctuations can affect the flow streamline, and eventually the blood-cell depletion and bead recovery. We therefore used a syringe pump to inject the reagents and buffer solution. The buffer was injected at a higher flow rate (75 µl min^{-1}) compared with the sample solution (15 µl min^{-1}), and this higher flow rate that comes from a syringe pump without any fluctuations helps maintain DLD function.

Binding kinetics measurement. The binding kinetics between insulin and the cAb were measured with biolayer interferometry using ForteBio Octet RED384 system. The cAb was biotinylated following the manufacturer's instructions for the EZ-Link NHS-PEG$_4$-biotin kit (Thermo Fisher) and then purified using Amicon Ultra centrifugal filter units (Millipore Sigma). Capture antibodies (100 nM) were loaded onto streptavidin biosensors (ForteBio) for 180 s, followed by 300 s baseline (in PBSBT), 500 s association and 360 s baseline steps. Association and dissociation were measured for insulin at concentrations of 1,500, 1,250, 1,000, 500, 250, 125, 62.5 and 0 nM. An additional experiment without cAb loading (insulin only) was performed as a control to account for non-specific insulin binding to the bare biosensors. The data were baseline aligned and then the background signal from the 0 nM insulin reference well and the corresponding insulin concentration for the unloaded probes experiment (insulin-only test) were subtracted to remove the background. Association and dissociation curves were then aligned and analysed using the association and dissociation kinetics nonlinear regression fit of GraphPad Prism 8 (Supplementary Fig. 18).

Reporting Summary. Further information on research design is available in the Nature Research Reporting Summary linked to this article.

Data availability

The data supporting the results in this study are available within the paper and its Supplementary Information. All raw and annotated data generated in this

study are available from figshare with the identifier https://doi.org/10.6084/m9.figshare.13218740.v1.

Code availability

The Python code used to analyse bead images is provided at https://github.com/beirami/rt-elisa.

Received: 23 January 2020; Accepted: 11 November 2020;
Published online: 21 December 2020

References

1. Hamburg, M. A. & Collins, F. S. The path to personalized medicine. *N. Engl. J. Med.* **363**, 301–304 (2010).
2. Puhr, S., Calhoun, P., Welsh, J. & Walker, T. The effect of reduced self-monitored blood glucose testing after adoption of continuous glucose monitoring on hemoglobin A1c and time in range. *Diabetes Technol. Ther.* **20**, 557–560 (2018).
3. Meuwese, C., Stenvinkel, P., Dekker, F. & Carrero, J. Monitoring of inflammation in patients on dialysis: forewarned is forearmed. *Nat. Rev. Nephrol.* **7**, 166–176 (2011).
4. Della Ciana, L. & Caputo, G. Robust, reliable biosensor for continuous monitoring of urea during dialysis. *Clin. Chem.* **42**, 1079–1085 (1996).
5. Nagler, R. M. Saliva analysis for monitoring dialysis and renal function. *Clin. Chem.* **54**, 1415–1417 (2008).
6. Pickering, J. W. et al. Rapid rule-out of acute myocardial infarction with a single high-sensitivity cardiac troponin T measurement below the limit of detection: a collaborative meta-analysis. *Ann. Intern. Med.* **166**, 715–724 (2017).
7. Hovorka, R. Continuous glucose monitoring and closed-loop systems. *Diabet. Med.* **23**, 1–12 (2006).
8. Baker, D. A. & Gough, D. A. A continuous, implantable lactate sensor. *Anal. Chem.* **67**, 1536–1540 (1995).
9. Khan, Y. et al. A flexible organic reflectance oximeter array. *Proc. Natl Acad. Sci. USA* **115**, E11015–E11024 (2018).
10. Ferguson, B. S. et al. Real-time, aptamer-based tracking of circulating therapeutic agents in living animals. *Sci. Transl. Med.* **5**, 213ra165 (2013).
11. Arroyo-currás, N. et al. Real-time measurement of small molecules directly in awake, ambulatory animals. *Proc. Natl Acad. Sci. USA* **114**, 645–650 (2017).
12. Navaneelan, T., Alam, S., Peters, P. A. & Phillips, O. Deaths involving sepsis in Canada. *Health at a Glance* (21 July 2016).
13. Garg, S. K., Rewers, A. H. & Akturk, H. K. Ever-increasing insulin-requiring patients globally. *Diabetes Technol. Ther.* **20**, S21–S24 (2018).
14. *Diabetes: Key Facts* (World Health Organization, 2018); https://www.who.int/news-room/fact-sheets/detail/diabetes
15. Basu, S. et al. Estimation of global insulin use for type 2 diabetes, 2018–30: a microsimulation analysis. *Lancet Diabetes Endocrinol.* **7**, 25–33 (2019).
16. Casparie, A. F. & Elving, L. D. Severe hypoglycemia in diabetic patients: frequency, causes, prevention. *Diabetes Care* **8**, 141–145 (1985).
17. Cryer, P., Davis, S. & Shamoon, H. Hypoglycemia in diabetes. *Diabetes Care* **26**, 1902–1912 (2003).
18. Geller, A. et al. National estimates of insulin-related hypoglycemia and errors leading to emergency department visits and hospitalizations. *JAMA Intern. Med.* **174**, 678–686 (2014).
19. Guerci, B. & Sauvanet, J. P. Subcutaneous insulin: pharmacokinetic variability and glycemic variability. *Diabetes Metab.* **31**, 7–24 (2005).
20. Gin, H. & Hanaire-Broutin, H. Reproducibility and variability in the action of injected insulin. *Diabetes Metab.* **31**, 7–13 (2005).
21. Heinemann, L. Variability of insulin absorption and insulin action. *Diabetes Technol. Ther.* **4**, 673–682 (2002).
22. Wilson, B. D., Hariri, A. A., Thompson, I. A. P. & Eisenstein, M. Independent Control of the thermodynamic and kinetic properties of aptamer switches. *Nat. Commun.* **10**, 5079 (2019).
23. Tang, Z. et al. Aptamer switch probe based on intramolecular displacement. *J. Am. Chem. Soc.* **130**, 11268–11269 (2008).
24. Munzar, J. D., Ng, A. & Juncker, D. Duplexed aptamers: history, design, theory, and application to biosensing. *Chem. Soc. Rev.* **48**, 1390–1419 (2019).
25. Nakatsuka, N. et al. Aptamer-field-effect transistors overcome debye length limitations for small-molecule sensing. *Science* **362**, 319–324 (2019).
26. Li, J., Janle, E. & Campbell, W. W. Postprandial glycemic and insulinemic responses to common breakfast beverages consumed with a standard meal in adults who are overweight and obese. *Nutrients* **9**, 32 (2017).
27. Bantle, J. P. et al. Postprandial glucose and insulin responses to meals containing different carbohydrates in normal and diabetic subjects. *N. Engl. J. Med.* **309**, 7–12 (1983).
28. ter Braak, E. W. et al. Injection site effects on the pharmacokinetics and glucodynamics of insulin lispro and regular insulin. *Diabetes Care* **19**, 1437–1440 (1996).
29. Home, P. D. The pharmacokinetics and pharmacodynamics of rapid-acting insulin analogues and their clinical consequences. *Diabetes Obes. Metab.* **14**, 780–788 (2012).
30. Freckmann, G. et al. Continuous glucose profiles in healthy subjects under everyday life conditions and after different meals. *J. Diabetes Sci. Technol.* **1**, 695–703 (2007).
31. Meijer, H. E. H., Singh, M. K., Kang, T. G., Den Toonder, J. M. J. & Anderson, P. D. Passive and active mixing in microfluidic devices. *Macromol. Symp.* **279**, 201–209 (2009).
32. Marschewski, J. et al. Mixing with herringbone-inspired microstructures: overcoming the diffusion limit in co-laminar microfluidic devices. *Lab Chip* **15**, 1923–1933 (2015).
33. Paek, S. H., Lee, S. H., Cho, J. H. & Kim, Y. S. Development of rapid one-step immunochromatographic assay. *Methods* **22**, 53–60 (2000).
34. Pollema, C. H., Ruzicka, J., Christian, G. D., Lernmark, A. & Lernmark, A. Sequential injection immunoassay utilizing immunomagnetic beads. *Anal. Chem.* **64**, 1356–1361 (1992).
35. Chang, L. et al. Single molecule enzyme-linked immunosorbent assays: theoretical considerations. *J. Immunol. Methods* **378**, 102–115 (2012).
36. McGrath, J., Jimenez, M. & Bridle, H. Deterministic lateral displacement for particle separation: a review. *Lab Chip* **14**, 4139–4158 (2014).
37. Gomis, S. et al. Single-cell tumbling enables high-resolution size profiling of retinal stem cells. *ACS Appl. Mater. Interfaces* **10**, 34811–34816 (2018).
38. Peiris, H. et al. Discovering human diabetes-risk gene function with genetics and physiological assays. *Nat. Commun.* **9**, 3855 (2018).
39. Adolfsson, P., Parkin, C. G., Thomas, A. & Krinelke, L. G. Selecting the appropriate continuous glucose monitoring system—a practical approach. *Eur. Endocrinol.* **14**, 24–29 (2018).
40. Wu, K. & Huan, Y. Streptozotocin-induced diabetic models in mice and rats. *Curr. Protoc. Pharm.* **5**, 5.47.1–5.47.20 (2008).
41. *Humulin R* (Eli Lilly and Company, 2018); https://www.accessdata.fda.gov/drugsatfda_docs/label/2011/018780s120lbl.pdf
42. *Humulin N* (Eli Lilly and Company, 2018); https://www.accessdata.fda.gov/drugsatfda_docs/label/2013/018781s121lbl.pdf
43. Woodworth, J. R., Howey, D. C. & Bowsher, R. R. Establishment of time-action profiles for regular and NPH insulin using pharmacodynamic modeling. *Diabetes Care* **17**, 64–68 (1994).
44. Kim, J., Campbell, A. S., De Ávila, B. E. F. & Wang, J. Wearable biosensors for healthcare monitoring. *Nat. Biotechnol.* **37**, 389–406 (2019).
45. Munje, R. D., Muthukumar, S., Jagannath, B. & Prasad, S. A new paradigm in sweat based wearable diagnostics biosensors using room temperature ionic liquids (RTILs). *Sci. Rep.* **7**, 1950 (2017).
46. Hao, Z. et al. Measurement of cytokine biomarkers using an aptamer-based affinity graphene nanosensor on a flexible substrate toward wearable applications. *Nanoscale* **10**, 21681–21688 (2018).
47. Visser, E. W. A., Yan, J., Van IJzendoorn, L. J. & Prins, M. W. J. Continuous biomarker monitoring by particle mobility sensing with single molecule resolution. *Nat. Commun.* **9**, 2541 (2018).
48. Goodwin, M. L., Harris, J. E., Hernández, A. & Gladden, L. B. Blood lactate measurements and analysis during exercise: A guide for clinicians. *J. Diabetes Sci. Technol.* **1**, 558–569 (2007).
49. Graf, A. et al. Moving toward a unified platform for insulin delivery and sensing of inputs relevant to an artificial pancreas. *J. Diabetes Sci. Technol.* **11**, 308–314 (2017).
50. Wiesli, P. et al. Acute psychological stress affects glucose concentrations in patients with type 1 diabetes following food intake but not in the fasting state. *Diabetes Care* **28**, 1910–1915 (2005).

Acknowledgements

This research was supported by the Chan Zuckerberg Biohub, a Stanford Diabetes Research Center (SDRC) Pilot grant and the Transdisciplinary Initiative Program (TIP) from the Stanford Maternal & Child Health Research Institute (MCHRI). C.L.M. was supported by a NSERC Postgraduate Scholarship and Stanford Bio-X Bowes Graduate Student Fellowship. We thank B. Buckingham and R. Lal for their helpful discussions as well as N. Maganzini and I. Thompson for their review and edits of the manuscript. We thank the Stanford Nanofabrication Facility (NSF) for their cleanroom facilities and the Canary Center at Stanford for Cancer Early Detection for their biolayer interferometry instrument. We thank the Stanford Veterinary Service Center staff for their assistance with animal care and procedures.

Author contributions

M.P., C.L.M. and H.T.S. conceived the initial concept. M.P. and C.L.M. designed experiments. M.P., C.L.M., E.Y.M., J.P., D.M., Y.H., A.Y. and S.W.B. executed experiments. A.B. developed the imaging analysis algorithm. M.P. and C.L.M. analysed the data. M.P., C.L.M., M.E. and H.T.S. wrote the manuscript. All authors edited, discussed and approved the whole paper.

Competing interests
The authors declare no competing interests.

Additional information
Supplementary information is available for this paper at https://doi.org/10.1038/s41551-020-00661-1.

Correspondence and requests for materials should be addressed to E.A.A. or H.T.S.

nature research

Corresponding author(s): Eric Appel and Tom Soh

Reporting Summary

Nature Research wishes to improve the reproducibility of the work that we publish. This form provides structure for consistency and transparency in reporting. For further information on Nature Research policies, see Authors & Referees and the Editorial Policy Checklist.

Statistical parameters

When statistical analyses are reported, confirm that the following items are present in the relevant location (e.g. figure legend, table legend, main text, or Methods section).

n/a	Confirmed	
☐	☒	The exact sample size (*n*) for each experimental group/condition, given as a discrete number and unit of measurement
☐	☒	An indication of whether measurements were taken from distinct samples or whether the same sample was measured repeatedly
☐	☒	The statistical test(s) used AND whether they are one- or two-sided *Only common tests should be described solely by name; describe more complex techniques in the Methods section.*
☒	☐	A description of all covariates tested
☒	☐	A description of any assumptions or corrections, such as tests of normality and adjustment for multiple comparisons
☐	☒	A full description of the statistics including central tendency (e.g. means) or other basic estimates (e.g. regression coefficient) AND variation (e.g. standard deviation) or associated estimates of uncertainty (e.g. confidence intervals)
☐	☒	For null hypothesis testing, the test statistic (e.g. *F*, *t*, *r*) with confidence intervals, effect sizes, degrees of freedom and *P* value noted *Give P values as exact values whenever suitable.*
☒	☐	For Bayesian analysis, information on the choice of priors and Markov chain Monte Carlo settings
☒	☐	For hierarchical and complex designs, identification of the appropriate level for tests and full reporting of outcomes
☒	☐	Estimates of effect sizes (e.g. Cohen's *d*, Pearson's *r*), indicating how they were calculated
☐	☒	Clearly defined error bars *State explicitly what error bars represent (e.g. SD, SE, CI)*

Our web collection on statistics for biologists may be useful.

Software and code

Policy information about availability of computer code

Data collection	No software was used.
Data analysis	GraphPad Prism 6 (GraphPad Software) was used for statistical analysis. A custom code written in Python (https://github.com/beirami/rt-elisa) was used to measure bead intensity.

For manuscripts utilizing custom algorithms or software that are central to the research but not yet described in published literature, software must be made available to editors/reviewers upon request. We strongly encourage code deposition in a community repository (e.g. GitHub). See the Nature Research guidelines for submitting code & software for further information.

Data

Policy information about availability of data

All manuscripts must include a data availability statement. This statement should provide the following information, where applicable:

- Accession codes, unique identifiers, or web links for publicly available datasets
- A list of figures that have associated raw data
- A description of any restrictions on data availability

The data supporting the results in this study are available within the paper and its Supplementary Information. All raw and annotated data generated in this study are available from figshare with the identifier https://doi.org/10.6084/m9.figshare.13218740.v1.

Field-specific reporting

Please select the best fit for your research. If you are not sure, read the appropriate sections before making your selection.

☒ Life sciences ☐ Behavioural & social sciences ☐ Ecological, evolutionary & environmental sciences

For a reference copy of the document with all sections, see nature.com/authors/policies/ReportingSummary-flat.pdf

Life sciences study design

All studies must disclose on these points even when the disclosure is negative.

Sample size	Experiments were used as proof-of-concept examples, and thus sample size was n = 1.
Data exclusions	No data were excluded.
Replication	Experiments were performed over multiple days with different devices. Different rats were used for each experiment.
Randomization	Rats were selected arbitrarily for the experiments.
Blinding	Blinding was not relevant.

Reporting for specific materials, systems and methods

Materials & experimental systems

n/a	Involved in the study
☒	☐ Unique biological materials
☐	☒ Antibodies
☒	☐ Eukaryotic cell lines
☒	☐ Palaeontology
☐	☒ Animals and other organisms
☒	☐ Human research participants

Methods

n/a	Involved in the study
☒	☐ ChIP-seq
☒	☐ Flow cytometry
☒	☐ MRI-based neuroimaging

Antibodies

Antibodies used	Matched paired insulin antibodies (capture: BM364-Z8A2, detection: BM364-T8F5) were obtained from BBI Solutions.
Validation	Insulin antibodies were validated using a benchtop bead-based assay for using in the RT-ELISA device.

Animals and other organisms

Policy information about studies involving animals; ARRIVE guidelines recommended for reporting animal research

Laboratory animals	Male Sprague Dawley rats (from Charles River) 8–10 weeks old and weighing 200–300 g at the start of the experiment.
Wild animals	The study did not involve wild animals.
Field-collected samples	The study did not involve samples collected from the field.